

## MATHEMATICAL ANALYSIS OF AG-TiO<sub>2</sub>/BLOOD HYBRID NANOFLUID WITH INCLUSION OF VISCOUS DISSIPATION OVER A PERMEABLE SURFACE

(Analisis Matematik Nanobendalir Hibrid Ag-TiO<sub>2</sub>/Darah dengan Lesapan Likat  
Terhadap Permukaan Telap)

RAHIMAH JUSOH\*, MUHAMMAD KHAIRUL ANUAR MOHAMED & MOHD HISYAM ARIFF

### ABSTRACT

The remarkable efficiency of hybrid nanofluids in heat transfer has made them a prominent research topic. This study investigates the boundary layer flow and heat transfer of Ag-TiO<sub>2</sub>/blood hybrid nanofluid while taking viscous dissipation into account. The governing partial differential equations of the hybrid nanofluid are transformed into ordinary differential equations using the requisite similarity transformations. The *bvp4c* function is then used in Matlab to generate numerical and graphical output. The accurate initial guessing values are then used to calculate the dual solutions. The existence of viscous dissipation considerably reduces the rate of heat transfer in this model. The effects of nanoparticle concentration have also been studied. The thickness of the boundary layer diminishes as the suction parameter rises, whereas different patterns of results are obtained as the concentration of argentum and titania nanoparticles changes.

*Keywords:* hybrid nanofluid; viscous dissipation; dual solutions

### ABSTRAK

Keberkesanan nanobendalir hibrid yang menakjubkan dalam pemindahan haba menjadikannya topik kajian yang utama. Penyelidikan ini mengkaji aliran lapisan sempadan dan pemindahan haba nanobendalir hibrid Ag-TiO<sub>2</sub>/darah dengan mempertimbangkan kesan lesapan likat. Persamaan pembezaan separa bagi nanobendalir hibrid ditukarkan kepada persamaan pembezaan biasa dengan menggunakan penjelmaan keserupaan. Kemudian fungsi *bvp4c* dalam Matlab digunakan untuk menjana keputusan berangka dan grafik. Nilai-nilai tekaan awal yang tepat pula digunakan untuk mendapatkan penyelesaian dual. Kewujudan lesapan likat mengurangkan kadar pemindahan haba di dalam model ini. Kesan kepekatan nanozarah turut dikaji. Ketebalan lapisan sempadan semakin berkurangan dengan peningkatan sedutan, manakala corak hasil kajian yang berbeza-beza diperolehi apabila kepekatan nanozarah argentum dan titania berubah.

*Kata kunci:* nanobendalir hibrid; lesapan likat; penyelesaian dual

## 1. Introduction

The field of nanotechnology has garnered much attention from academics, who have been utilizing nanofluids in both experimental and theoretical research. The increasing focus on nanofluids is a result of the recognition that using conventional fluids as a means of heat transfer has its limitations. Choi and Eastman (1995) theorized that adding nanoparticles can enhance heat conductivity in their study. Nanofluids have a range of applications in industries, technology, and biology, such as drug delivery, cooling microchips, hybrid engines, cancer treatment, geothermal power generation, and industrial cooling. Recently,

researchers have been focusing on a new type of nanofluid called hybrid nanofluids, which involves combining two or more nanoparticles to enhance the heat transfer properties of nanofluids. Benedict *et al.* (2020) proved that the combination of aluminium oxide and nanocellulose hybrid nanofluid could increase the performance of radiator coolant. An experimental study conducted by Vårdaru *et al.* (2023) showed that hybrid nanofluids containing argentum-reduced graphene oxide could lead to an improvement of 11% in thermal conductivity.

Apart from water, ethylene glycol, oil, and surfactant-stabilized fluids, blood also can be considered the base fluid for the hybrid nanofluid model. The flow characteristics and mechanical properties of blood can be studied using a modified version of the Darcy and Brinkman equation, providing a comprehensive understanding of diseases related to the human body and the development of improved artificial organs. Blood exhibits abnormal viscous properties due to the suspension of particles in plasma, and it is considered a non-Newtonian fluid at low shear rates and a Newtonian fluid at high shear rates when flowing through large arteries (Reddy *et al.* 2018). This information can assist bioengineers in their design and manufacturing of artificial organs and in finding solutions to human body-related diseases and disorders.

One aspect that can be taken into account in analyzing the flow and heat transfer of hybrid nanofluids is the factor of viscous dissipation. It is denoted by the Eckert number which refers to the transformation of mechanical energy into thermal energy due to internal friction within a fluid. It influences the temperature and thickness of the thermal boundary layer and can impact the overall heat transfer and energy efficiency of the system. Muhammad *et al.* (2021) conducted a numerical analysis of SWCNTs-CuO hybrid nanofluid and found that the enlargement of viscous dissipation raised the temperature. A similar finding also had been obtained by Kho *et al.* (2023) for the Ag-TiO<sub>2</sub> hybrid nanofluid model.

Furthermore, the convective boundary condition is also significant when exploring the heat transfer of hybrid nanofluid. It refers to the type of boundary at which heat transfer occurs from a solid surface to a fluid or from a fluid to a solid surface through convection. This type of boundary condition is important to understand the behavior of the fluid near the surface. The level of convective boundary condition is measured by the value of Biot number. Waini *et al.* (2019) and Zainal *et al.* (2020) considered convective boundary condition in their hybrid nanofluid research. They reached the conclusion that as the Biot number increases, the surface temperature rises and the thermal boundary layer becomes wider for both branches (dual solutions).

This present study is inspired by the previous investigations into the potential of hybrid nanofluids as an exceptional heat transfer medium. The hybrid nanofluid in this particular study is comprised of a mixture of silver or argentum nanoparticles (Ag) and titania (TiO<sub>2</sub>) nanoparticles, with blood serving as the base fluid. In order to accurately model the hybrid nanofluid, the impacts of viscous dissipation and convective boundary conditions are also considered and taken into account. This study highlights the importance of understanding the behavior of the thermal boundary layer in hybrid nanofluids, which can aid in optimizing their performance and improving their energy efficiency.

## 2. Problem Formulations

In this section, the readers will have a firm grasp of the study's foundational parameters. The work began with the identification of the physical model of the two-dimensional Ag-TiO<sub>2</sub>/blood hybrid nanofluid. Figure 1 depicts the coordinate system and model configuration of the hybrid nanofluid. A rectangular coordinate frame is used, with the surface being

stretched/shrunk so that it is parallel to the  $x$ -axis and the  $y$ -axis being orthogonal to the surface. It is presumable that the surface is permeable with  $v_w$  as the mass flux velocity. Besides, the permeable surface is stretched ( $\lambda > 0$ ) and shrunk ( $\lambda < 0$ ) with the velocity  $u = \lambda u_w(x)$ . In addition, the hot fluid at temperature  $T_f = T_\infty + bx^2$  with dimensionless constant  $b$  and correlates to the heat transfer coefficient  $h_f$  heated the bottom surface convectively.

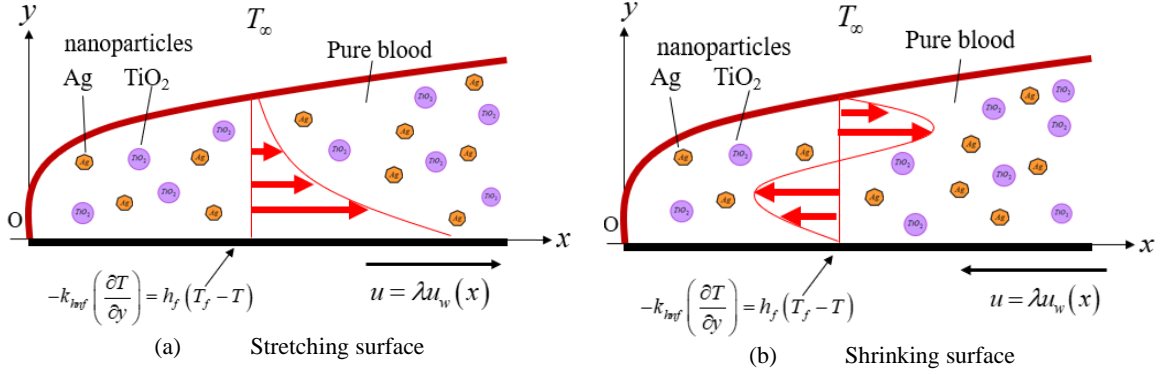


Figure 1: Physical configuration of Ag-TiO<sub>2</sub>/blood hybrid nanofluid

The fundamental equations of boundary layer flow of Ag-TiO<sub>2</sub>/blood hybrid nanofluid which incorporates the continuity, momentum and energy are described as follows:

$$\frac{\partial u}{\partial x} + \frac{\partial v}{\partial y} = 0, \quad (1)$$

$$u \frac{\partial u}{\partial x} + v \frac{\partial u}{\partial y} = \frac{\mu_{hnf}}{\rho_{hnf}} \frac{\partial^2 u}{\partial y^2}, \quad (2)$$

$$u \frac{\partial T}{\partial x} + v \frac{\partial T}{\partial y} = \alpha_{hnf} \frac{\partial^2 T}{\partial y^2} + \frac{\mu_{hnf}}{(\rho C_p)_{hnf}} \left( \frac{\partial u}{\partial y} \right)^2. \quad (3)$$

subject to the satisfaction of certain boundary conditions

$$u = \lambda u_w(x) = \lambda ax, \quad v = v_w, \quad -k_{hnf} \left( \frac{\partial T}{\partial y} \right) = h_f (T_f - T) \text{ at } y = 0, \quad (4)$$

$$u \rightarrow 0, \quad T \rightarrow T_\infty \quad \text{as } y \rightarrow \infty.$$

In the aforementioned equations,  $u$  and  $v$  exemplifies the velocity components in  $x$  – and  $y$  – directions, respectively with the positive constant  $a$  while  $T$  implies the temperature of the hybrid nanofluid. The additional parameters that portrays the thermophysical properties of the hybrid nanofluid are  $k_{hnf}$ ,  $\mu_{hnf}$ ,  $\rho_{hnf}$ ,  $\alpha_{hnf}$ , and  $(\rho C_p)_{hnf}$  which embody the thermal conductivity, dynamic viscosity, density, thermal diffusivity and heat capacity, respectively. Table 1 contains the formulae for the hybrid nanofluid characteristics. The argentum nanoparticles are signified by subscript s1 in the table, while the titanium dioxide or titania nanoparticles are indicated by subscript s2. On the other hand, the subscript  $f$  represents the base fluid (blood),  $nf$  stands for the nanofluid, and  $hnf$  for the hybrid nanofluid. Within the context of this

research, blood is modelled as a viscous, incompressible fluid. For purposes of reference, Table 2 lists the thermophysical attributes of the blood as well as the argentum and titania nanoparticles.

Table 1: Formulations of hybrid nanofluid properties

Properties	Nanofluid	Hybrid nanofluid
Density	$\rho_{nf} = (1 - \phi_1)\rho_f + \phi_1\rho_s$	$\rho_{hnf} = (1 - \phi_2)\left[(1 - \phi_1)\rho_f + \phi_1\rho_{s1}\right] + \phi_2\rho_{s2}$
Heat capacity	$(\rho C_p)_{nf} = (1 - \phi_1)(\rho C_p)_f + \phi_1(\rho C_p)_{s1}$	$(\rho C_p)_{hnf} = (1 - \phi_2)\left[\frac{(1 - \phi_1)(\rho C_p)_f}{+ \phi_1(\rho C_p)_{s1}}\right] + \phi_2(\rho C_p)_{s2}$
Dynamic viscosity	$\mu_{nf} = \frac{\mu_f}{(1 - \phi_1)^{2.5}}$	$\mu_{hnf} = \frac{\mu_f}{(1 - \phi_1)^{2.5}(1 - \phi_2)^{2.5}}$
Thermal Conductivity	$k_{nf} = \frac{k_{s1} + 2k_f - 2\phi_1(k_f - k_{s1})}{k_{s1} + 2k_f + \phi_1(k_f - k_{s1})} \times k_f$	$k_{hnf} = \frac{k_{s2} + 2k_{nf} - 2\phi_2(k_{nf} - k_{s2})}{k_{s2} + 2k_{nf} + \phi_2(k_{nf} - k_{s2})} \times k_{nf}$ where $k_{nf} = \frac{k_{s1} + 2k_f - 2\phi_1(k_f - k_{s1})}{k_{s1} + 2k_f + \phi_1(k_f - k_{s1})} \times k_f$

Table 2: Pure blood and nanoparticles's thermophysical attributes (Benkhedda *et al.* 2018; Chahreg & Dinarvand 2020)

Properties	$\rho(kgm^{-3})$	$C_p(Jkg^{-1}K^{-1})$	$k(Wm^{-1}K^{-1})$
Argentum (Ag)	10500	235	429
Titanium Dioxide (TiO2)	4250	686.2	8.954
Pure Blood	1063	3594	0.492

The most practical approach for resolving the mathematical formulation of fluid mechanics is by using similarity transformation. It is useful in understanding the complex fluid flow with a physical explanation to the actual problem in addition to offering asymptotic solutions. Therefore, the following similarity transformations are used to simplify the governing Eqs. (1)-(3), which relate to the boundary conditions in Eq. (4):

$$u = axf'(\eta), \quad v = -\sqrt{av_f}f(\eta), \quad \eta = y\sqrt{\frac{a}{v_f}}, \quad \theta(\eta) = \frac{T - T_\infty}{T_f - T_\infty}. \quad (5)$$

Now, Eq. (1) is automatically fulfilled. Subsequently, Eqs. (2)-(3) are transformed into the following ordinary differential equations:

$$\frac{\mu_{hnf}/\mu_f}{\rho_{hnf}/\rho_f} f''' + ff'' - f'^2 = 0, \quad (6)$$

$$\frac{k_{hnf}/k_f}{Pr(\rho C_p)_{hnf}/(\rho C_p)_f} \theta'' + f\theta' - 2f'\theta + \frac{Ec}{(1 - \phi_1)^{2.5}(1 - \phi_2)^{2.5}(\rho C_p)_{hnf}/(\rho C_p)_f} f'^2 = 0, \quad (7)$$

based on the boundary conditions

$$\begin{aligned} f(0) = s, \quad f'(0) = \lambda, \quad \theta'(0) = -\frac{k_f}{k_{hnf}} Bi(1 - \theta(0)), \\ f'(\infty) \rightarrow 0, \quad \theta(\infty) \rightarrow 0. \end{aligned} \quad (8)$$

In this work, we focus on the permeable surface with positive value of  $s$ , which corresponds to the suction. In the meantime,  $Pr$  signifies the Prandtl number. We also consider the convective boundary condition with  $Bi$  as the Biot number and the viscous dissipation which exemplified by  $Ec$ . These parameters are formulated as

$$Pr = \frac{\nu_f}{\alpha_f}, \quad s = -\frac{v_w}{\sqrt{av_f}}, \quad Ec = \frac{u_w^2}{(C_p)_f(T_f - T_\infty)}, \quad Bi = h_f \sqrt{v_f/a} / k_f. \quad (9)$$

The formula of the skin friction coefficients  $C_f$ , the local Nusselt number  $Nu_x$  and the heat flux  $q_w$  are presented as

$$C_f = \frac{\mu_{hnf}}{\rho_f u_w^2} \left( \frac{\partial u}{\partial y} \right)_{y=0}, \quad Nu_x = \frac{x q_w}{k_f (T_w - T_\infty)}, \quad q_w = -k_{hnf} \left( \frac{\partial T}{\partial y} \right)_{y=0}. \quad (10)$$

Subsequently, we get

$$C_f Re_x^{1/2} = \frac{f''(0)}{(1 - \phi_1)^{2.5} (1 - \phi_2)^{2.5}}, \quad Nu_x Re_x^{-1/2} = -\frac{k_{hnf}}{k_f} \theta'(0), \quad (11)$$

where  $Re_x = \frac{u_w x}{\nu_f}$  symbolizes the local Reynolds number.

### 3. Stability Analysis

Stability analysis is essential for determining if the obtained solutions are technically stable. Initially, the unsteady case for Eqs. (2) and (3) must be considered as recommended by Merkin (1986), which can be formulated as

$$\frac{\partial u}{\partial t} + u \frac{\partial u}{\partial x} + v \frac{\partial u}{\partial y} = \frac{\mu_{hnf}}{\rho_{hnf}} \frac{\partial^2 u}{\partial y^2} - \frac{\sigma_{hnf} B_0^2}{\rho_{hnf}} u, \quad (12)$$

$$\frac{\partial T}{\partial t} + u \frac{\partial T}{\partial x} + v \frac{\partial T}{\partial y} = \alpha_{hnf} \frac{\partial^2 T}{\partial y^2} - \frac{1}{(\rho C_p)_{hnf}} \frac{\partial q_r}{\partial y}, \quad (13)$$

where  $t$  is referred to the time. Weidman *et al.* (2006) stated that a new dimensionless time variable  $\tau$  is crucial for stability analysis. Accordingly, the following new similarity transformations are used (Kho *et al.* 2022):

$$\begin{aligned}
 u &= ax \frac{\partial f}{\partial \eta}(\eta, \tau), & v &= -\sqrt{av_f} f(\eta, \tau), \\
 \theta(\eta, \tau) &= \frac{T - T_\infty}{T_f - T_\infty}, & \eta &= \sqrt{\frac{a}{\nu_f}} y, & \tau &= at.
 \end{aligned} \tag{14}$$

Implementation of similarity variables in Eq. (14) into Eqs. (12) and (13) leads to the generation of the following equations

$$\frac{\mu_{hmf} / \mu_f}{\rho_{hmf} / \rho_f} \frac{\partial^3 f}{\partial \eta^3} + f \frac{\partial^2 f}{\partial \eta^2} - \left( \frac{\partial f}{\partial \eta} \right)^2 - \frac{\partial^2 f}{\partial \eta \partial \tau} = 0, \tag{15}$$

$$\frac{k_{hmf} / k_f}{Pr(\rho C_p)_{hmf} / (\rho C_p)_f} \frac{\partial^2 \theta}{\partial \eta^2} + f \frac{\partial \theta}{\partial \eta} - 2 \frac{\partial f}{\partial \eta} \theta + \tag{16}$$

$$\frac{Ec}{(1-\phi_1)^{2.5} (1-\phi_2)^{2.5} (\rho C_p)_{hmf} / (\rho C_p)_f} \left( \frac{\partial^2 f}{\partial \eta^2} \right)^2 - \frac{\partial \theta}{\partial \tau} = 0,$$

associated with the boundary conditions

$$\begin{aligned}
 f(0, \tau) &= s, & \frac{\partial f}{\partial \eta}(0, \tau) &= \lambda, & \frac{\partial \theta}{\partial \eta}(0, \tau) &= -\frac{k_f}{k_{hmf}} Bi(1 - \theta(0, \tau)), \\
 \frac{\partial f}{\partial \eta}(\infty, \tau) &\rightarrow 0, & \theta(\infty, \tau) &\rightarrow 0.
 \end{aligned} \tag{17}$$

To assure the stability characteristic, the essential flow  $f = f_0(\eta)$  and  $\theta = \theta_0(\eta)$  are agitated by the exponential form of perturbation functions as follows (Arif *et al.* 2022):

$$f(\eta, \tau) = f_0(\eta) + e^{-\gamma\tau} F(\eta), \quad \theta(\eta, \tau) = \theta_0(\eta) + e^{-\gamma\tau} H(\eta), \tag{18}$$

with the unspecified eigenvalue parameter  $\gamma$  which portrays the growth/decay rate of agitations. It is worth mentioning that  $F(\eta)$  and  $H(\eta)$  are comparatively small to  $f_0(\eta)$  and  $\theta_0(\eta)$ . Then, the adaptation of perturbation function in Eq. (18) into Eqs. (15)-(17) generates the linearized equations as follows:

$$\frac{\mu_{hmf} / \mu_f}{\rho_{hmf} / \rho_f} F''' + f_0 F'' + F f_0'' - 2 f_0' F' + \gamma F' = 0, \tag{19}$$

$$\begin{aligned}
 &\frac{k_{hmf} / k_f}{Pr(\rho C_p)_{hmf} / (\rho C_p)_f} H'' + f_0 H' + F \theta_0' - 2 f_0' H - 2 F' \theta_0 + \gamma H \\
 &+ \frac{Ec}{(1-\phi_1)^{2.5} (1-\phi_2)^{2.5} (\rho C_p)_{hmf} / (\rho C_p)_f} (2 f_0'' F'') = 0
 \end{aligned} \tag{20}$$

correspond to

$$F(0) = 0, \quad F'(0) = 0, \quad H'(0) = \frac{k_f}{k_{mf}} BiH(0), \quad F'(\infty) \rightarrow 0, \quad H(\infty) \rightarrow 0. \quad (21)$$

A boundary condition as  $\eta$  approaches  $\infty$  must be loosened to generate the potential eigenvalues (Harris *et al.* 2009; Jamaludin *et al.* 2021; Najib *et al.* 2018). In this study, we choose the boundary condition  $F'(\infty) \rightarrow 0$  to be loosened. Hence, the stabilizing boundary condition  $F''(0) = 1$  is adapted to solve the system of equations in Eqs. (19)-(21).

#### 4. Results and Discussion

Exhaustive numerical simulations have been carried out using the `bvp4c` function in Matlab to provide a physical scrutiny on the flow problem. In order to validate the correctness and validity of the current study, current results for the skin friction coefficient are compared to those obtained by Makinde (2013) and Chaudary and Kanika (2019). In the previous study, Makinde (2013) applied the Runge-Kutta-Fehlberg method with shooting technique whereas Chaudary and Kanika (2019) utilized the Keller-Box method. In this comparison, we have set the Prandtl number as 6.2, as we are comparing the results for TiO<sub>2</sub>-water nanofluid. As depicted in Table 3, there is a high level of agreement in the comparisons, confirming the validity of the `bvp4c` function used in the study.

Table 3: Comparison of skin friction coefficient with variation in titanium dioxide nanoparticles concentration when  $Pr = 6.2$ ,  $\phi_1 = Ec = S = \lambda = 0$  and  $Bi = \infty$ .

$\phi_2$	Chaudary and Kanika (2019)	Makinde (2013)	Present Results
0	0.33258	0.3321	0.332096358
0.008	0.33350	0.3398	0.339794505
0.014	0.33410	0.3456	0.345629973
0.016	0.33430	0.3476	0.347587279
0.02	0.33466	0.3515	0.351520532
0.1	0.33569	0.4362	0.436277332
0.2	-	0.5642	0.564292593

This study provides insight into the relationship between various parameters such as viscous dissipation, Biot number, suction parameter and nanoparticle concentration with the flow and heat transfer behavior of the argentine-titania (Ag-TiO<sub>2</sub>) hybrid nanofluid. By following Chahregh and Dinarvand (2020), the Prandtl number is determined to be 21, as the base fluid used in the study is pure blood. The graphical results are illustrated in Figures 2-9, which show the impact of the governing parameters on the velocity profiles, temperature profiles, skin friction coefficient and the local Nusselt number.

The velocity gradient at the surface increases with an increase in suction, as shown in Figure 2. This increase in wall shear stress leads to a reduction in the thickness of the momentum boundary layer. On the other hand, Figure 3 shows that increased suction results in a decrease in the temperature distribution profile, leading to a thinning of the thermal boundary layer. This thinning of the thermal boundary layer enhances the process of heat transfer.

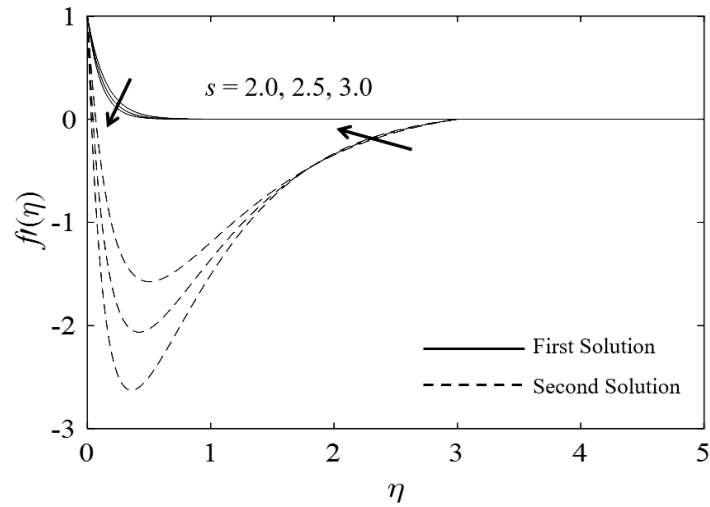


Figure 2: Changes of  $f'(\eta)$  for several  $s$  values when  $Ec = Bi = 1, Pr = 21, \phi_1 = \phi_2 = 0.02$  and  $\lambda = 1$

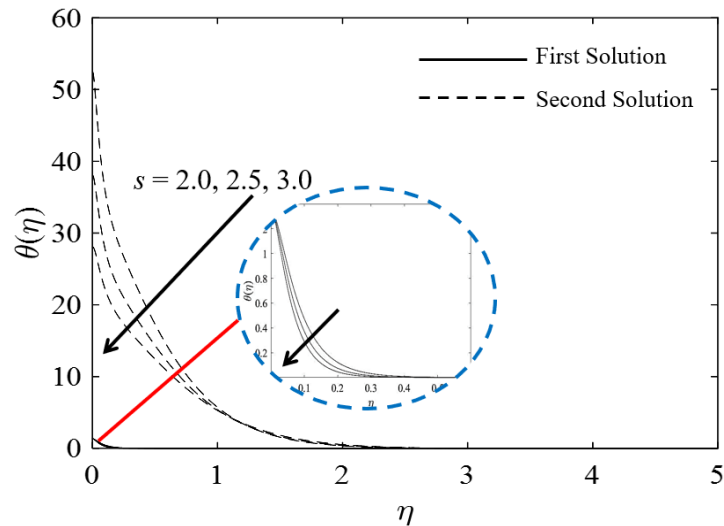


Figure 3: Changes of  $\theta(\eta)$  for several  $s$  values when  $Ec = Bi = 1, Pr = 21, \phi_1 = \phi_2 = 0.02$  and  $\lambda = 1$

The impact of viscous dissipation on the temperature profile of the hybrid nanofluid is depicted in Figure 4. The figure shows that the presence of viscous dissipation leads to an increase in the thickness of the thermal boundary layer. Viscous dissipation refers to the energy loss due to the friction between fluid layers in a fluid flow. This energy loss leads to a reduction in the rate of heat transfer, and as a result, the thermal boundary layer becomes thicker. In other words, the temperature gradient in the fluid becomes weaker, leading to a slower rate of heat transfer.

Likewise, the Biot number exhibits the same impact on the temperature profiles. Apparently, Figure 5 illustrates the growth of temperature profile as the Biot number boosts. The Biot number is defined as the ratio of the heat transfer rate by conduction to the rate of heat transfer by convection in a system. It ranges from zero to infinity, with values close to zero indicating that conduction dominates, and values close to infinity indicating that convection dominates. When the Biot number increases, it means that there is an increase in

the internal heat transfer resistance compared to the external heat transfer resistance. This results in a higher temperature at the surface and a wider thermal boundary layer, as more heat is being retained within the system.

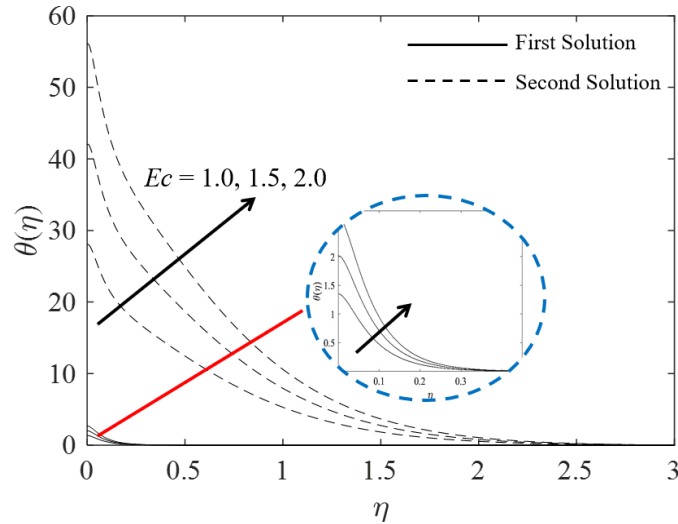


Figure 4: Changes of  $\theta(\eta)$  for several  $Ec$  values when  $s = 2, Bi = 1, Pr = 21, \phi_1 = \phi_2 = 0.02$  and  $\lambda = 1$

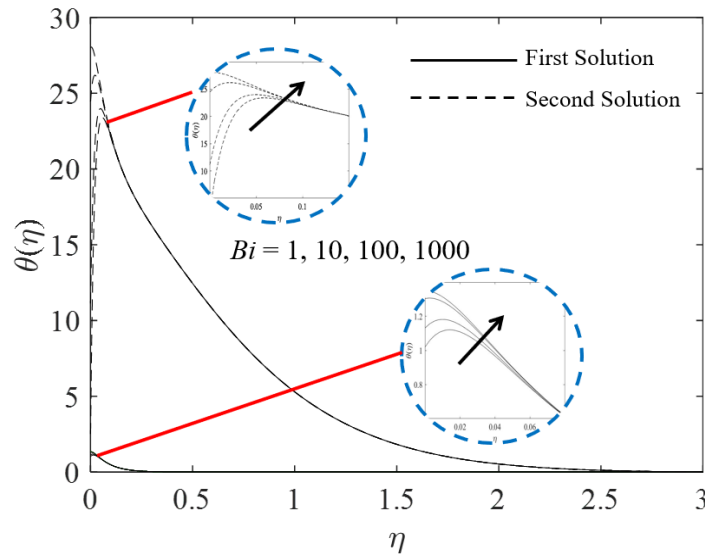


Figure 5: Changes of  $\theta(\eta)$  for several  $Bi$  values when  $s = 2, Ec = 1, Pr = 21, \phi_1 = \phi_2 = 0.02$  and  $\lambda = 1$

Figure 6 portrays the relationship between the local Nusselt number, which is a measure of the heat transfer rate, and the viscous dissipation parameter. Higher viscous dissipation causes a decrement of the local Nusselt number which reflecting the diminution rate of heat transfer. This can be attributed to the increase in the resistance to flow in the boundary layer, which reduces the convective heat transfer from the surface to the fluid. Similarly, Figure 7 also shows the decrement of local Nusselt number with a rise in the Biot number, which implies a reduction in the rate of heat transfer. Physically, Biot number represents the ratio of the internal thermal resistance to the external thermal resistance in a solid-fluid system. This

reduction occurs because an increase in the Biot number represents an increase in the internal thermal resistance, reducing the overall heat transfer efficiency of the system.

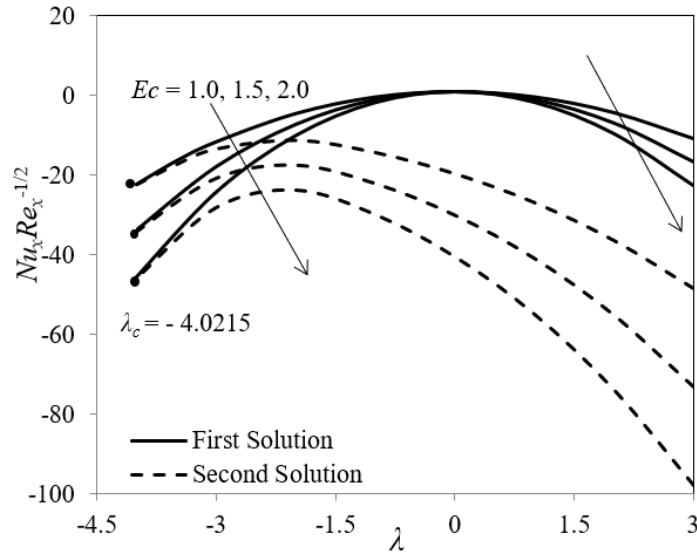


Figure 6: Changes of local Nusselt number for various  $Ec$  when  $s = 2$ ,  $Bi = 1$ ,  $\phi_1 = \phi_2 = 0.02$  and  $Pr = 21$

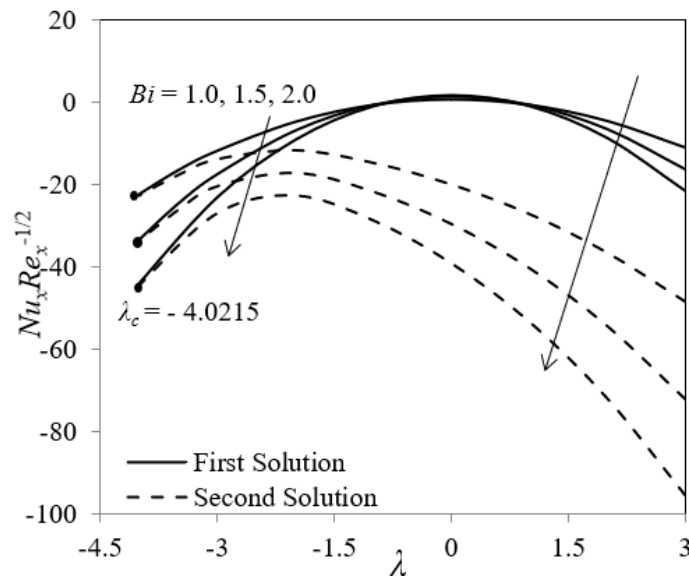


Figure 7: Changes of local Nusselt number for various  $Bi$  when  $s = 2$ ,  $Ec = 1$ ,  $\phi_1 = \phi_2 = 0.02$  and  $Pr = 21$

In addition, the implications of argementum nanoparticles volume fraction has also been analysed. Figure 8 exhibits that 0.5% higher concentration of argementum nanoparticles increase the skin friction coefficient, but different effect shown in Figure 9 where the local Nusselt number decreases. Intriguingly, Figure 8 reveals the presence of a non-unique solution when  $\lambda = 0$ , resulting in opposing flow up until the critical points  $\lambda_c$ . Clearly, the skin friction coefficient increases for the case of a shrinking surface ( $\lambda < 0$ ) and decreases when the

surface is stretched ( $\lambda > 0$ ). This finding aligns with the results obtained by Patel *et al.* (2023). An increase in the concentration of argentine nanoparticles results in a higher skin friction coefficient due to the enhanced interaction between the fluid and the nanoparticles at the wall. The increased skin friction coefficient can create a more turbulent flow, resulting in improved heat transfer. However, higher nanoparticle concentration can also lead to more inter-particle collisions and increased viscous dissipation, which can decrease the rate of heat transfer as illustrated in Figure 9. Therefore, a balance between these competing effects must be found to optimize the performance of the nanofluid for a specific application.

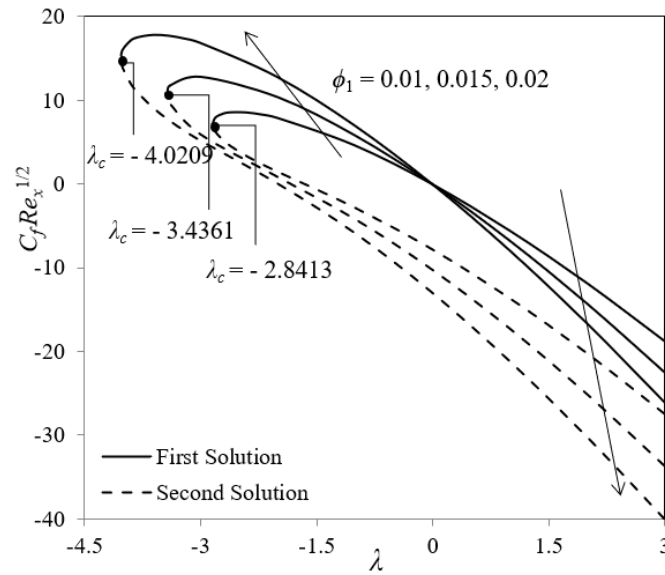


Figure 8: Impact of Ag nanoparticles to  $C_f Re_x^{1/2}$  when  $s = 2.5$ ,  $Ec = Bi = 1$ ,  $\phi_2 = 0.04$  and  $Pr = 21$

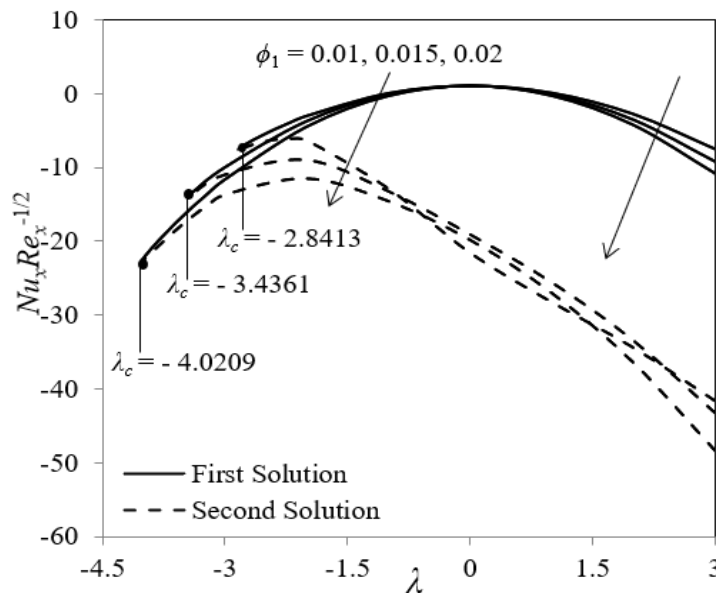


Figure 9: Impact of Ag nanoparticles to  $Nu_x Re_x^{-1/2}$  when  $s = 2.5$ ,  $Ec = Bi = 1$ ,  $\phi_2 = 0.04$  and  $Pr = 21$

In contrast, the impact of titania nanoparticle concentration on skin friction coefficient is delineated in Figure 10. It reveals that an increase of 2% in titania concentration leads to a decrease in skin friction. This discovery corresponds with the experimental investigation carried out by Birleanu *et al.* (2022) which proves that the addition of TiO<sub>2</sub> nanoparticles reduces the skin friction. The deposited TiO<sub>2</sub> nanoparticles on the surface serve as an additional layer, reducing the shear stress. These stable nanoparticles, compared to the debris generated by sliding, play a role in decreasing the skin friction. Subsequently, the reduction in skin friction caused by higher concentration of titania nanoparticles can affect the rate of heat transfer in a number of ways. This reduction in skin friction cause the fluid to move faster, altering the velocity profile and changing the rate of convection. Therefore, the higher concentration of titania nanoparticles can lead to a decrease in the rate of heat transfer as shown in Figure 11.

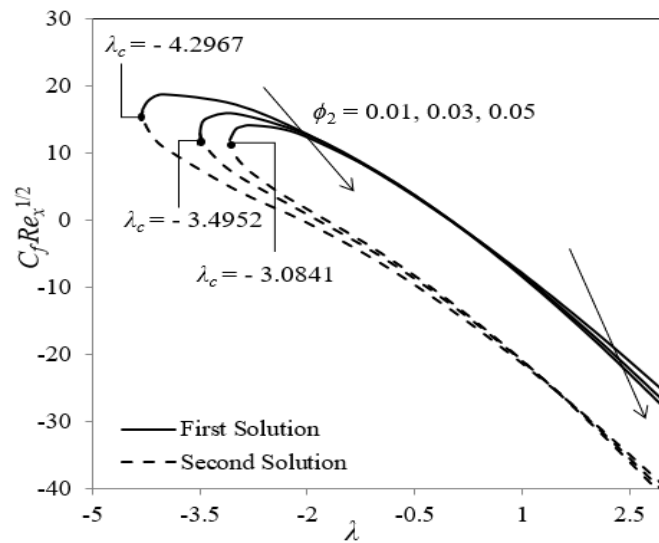


Figure 10: Impact of TiO<sub>2</sub> nanoparticles to  $C_f Re_x^{1/2}$  when  $s = 2.5$ ,  $Ec = Bi = 1$ ,  $\phi_1 = 0.02$  and  $Pr = 21$

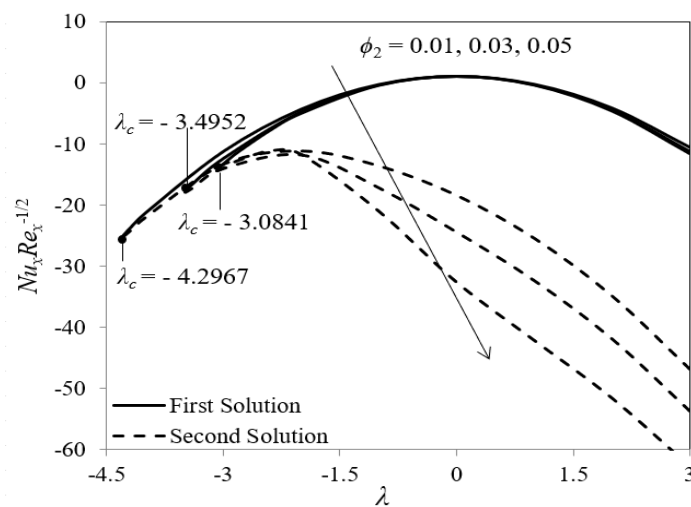


Figure 11: Impact of TiO<sub>2</sub> nanoparticles to  $Nu_x Re_x^{-1/2}$  when  $s = 2.5$ ,  $Ec = Bi = 1$ ,  $\phi_1 = 0.02$  and  $Pr = 21$

In order to assess the feasibility of the first and second solutions, a stability analysis is conducted. This is accomplished by solving the eigenvalue problems (19)-(21) and determining the minimum eigenvalue  $\gamma_1$ . A limitless set of eigenvalues  $\gamma_1 < \gamma_2 < \gamma_3 \dots$  is generated with the minimum eigenvalue being designated as  $\gamma_1$ . If the minimum eigenvalue is negative, it indicates an initial increase in disturbances and therefore instability in the flow. On the other hand, if the minimum eigenvalue is positive, it signals a decline in disturbances and stability in the flow. As shown in Figure 12, the first solution is determined to be stable, but the second solution is found to be unstable.

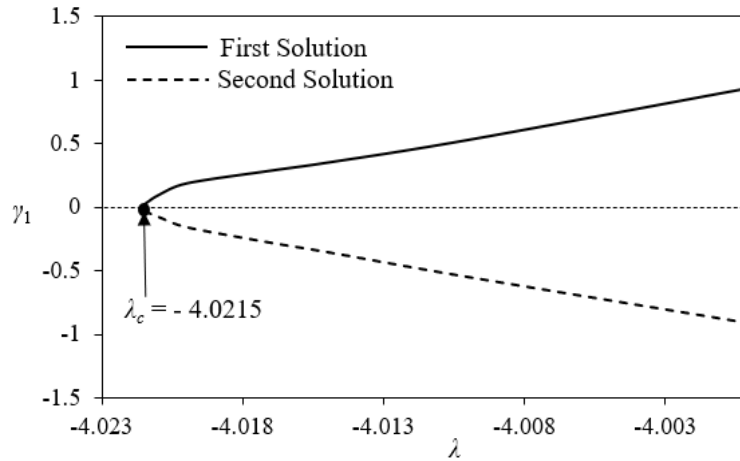


Figure 12: Variations of  $\gamma_1$  with  $\lambda$  when  $s = 2$ ,  $Bi = Ec = 1$ ,  $\phi_1 = \phi_2 = 0.02$  and  $Pr = 21$

## 5. Conclusions

This study presented the numerical analysis of the hybrid nanofluid flow in a laminar, isothermal and incompressible manner over a permeable surface that is either stretching or shrinking. The hybrid nanofluid was composed of two nanoparticles, TiO<sub>2</sub> and Ag, suspended in pure blood. The changes in velocity, temperature profile, wall shear stress, and local Nusselt number due to variations in the physical parameters were explored through graphical representation. The presence of suction led to an increase in the velocity distribution profile and a decrease in the thickness of the momentum boundary layer, while an increase in viscous dissipation led to an increase in temperature and a thickening of the thermal boundary layer. An increase in the Biot number resulted in an increase in the rate of convection, which in turn enlarges the thickness of the thermal boundary layer. It was also found that higher concentrations of argentum and titania nanoparticles reduced the rate of heat transfer. Therefore, further investigation is required to determine the optimal concentration of Ag and TiO<sub>2</sub> nanoparticles that enhance the heat transfer rate. From the stability analysis, it can be concluded that the first solution was considered stable, while the second solution was considered unstable. Further research involving hybrid nanofluids with blood as the base fluid can be explored, as they have various potential applications in the medical and biomedical fields due to their unique thermal and rheological properties.

## Acknowledgements

The authors extend their sincere appreciation to Universiti Malaysia Pahang for financing this work with research grants (RDU223202 and RDU213201).

## References

- Arif M., Suneetha S., Basha T., Anki Reddy P.B. & Kumam P. 2022. Stability analysis of diamond-silver-ethylene glycol hybrid based radiative micropolar nanofluid: A solar thermal application. *Case Studies in Thermal Engineering* **39**: 102407.
- Benedict F., Kumar A., Kadirgama K., Mohammed H.A., Ramasamy D., Samykano M. & Saidur R. 2020. Thermal performance of hybrid-inspired coolant for radiator application. *Nanomaterials* **10**(6): 1100.
- Benkhedda M., Boufendi T. & Touahri S. 2018. Laminar mixed convective heat transfer enhancement by using Ag-TiO<sub>2</sub>-water hybrid Nanofluid in a heated horizontal annulus. *Heat and Mass Transfer/Waerme- Und Stoffuebertragung* **54**(9): 2799–2814.
- Birleanu C., Pustan M., Cioaza M., Molea A., Popa F. & Contiu G. 2022. Effect of TiO<sub>2</sub> nanoparticles on the tribological properties of lubricating oil: an experimental investigation. *Scientific Reports* **12**: 5201.
- Chahregheh H.S. & Dinarvand S. 2020. TiO<sub>2</sub>-Ag/blood hybrid nanofluid flow through an artery with applications of drug delivery and blood circulation in the respiratory system. *International Journal of Numerical Methods for Heat and Fluid Flow* **30**(11): 4775–4796.
- Chaudhary S. & Kanika K. 2019. Impacts of viscous dissipation and Joule heating on hydromagnetic boundary layer flow of nanofluids over a flat surface subjected to Newtonian heating. *SN Applied Sciences* **1**: 1709.
- Choi S.U.S. & Eastman J.A. 1995. Enhancing thermal conductivity of fluids with nanoparticles. *The Proceedings of the 1995 ASME International Mechanical Engineering Congress and Exposition* **66**: 99–105.
- Harris S.D., Ingham D.B. & Pop I. 2009. Mixed convection boundary-layer flow near the stagnation point on a vertical surface in a porous medium: Brinkman model with slip. *Transport in Porous Media* **77**: 267–285.
- Jamaludin A., Nazar R., Naganthran K. & Pop I. 2021. Mixed convection hybrid nanofluid flow over an exponentially accelerating surface in a porous media. *Neural Computing and Applications* **33**: 5719–15729.
- Kho Y.B., Jusoh R., Salleh M.Z., Ariff M.H. & Zainuddin N. 2022. Magnetohydrodynamics Ag-Fe<sub>3</sub>O<sub>4</sub>-Ethylene Glycol hybrid nanofluid flow and heat transfer with thermal radiation. *CFD Letters* **14**(11): 88–101.
- Kho Y.B., Jusoh R., Salleh M.Z., Ariff M.H. & Zainuddin N. 2023. Magnetohydrodynamics flow of Ag-TiO<sub>2</sub> hybrid nanofluid over a permeable wedge with thermal radiation and viscous dissipation. *Journal of Magnetism and Magnetic Materials* **565**: 170284.
- Makinde O.D. 2013. Effects of viscous dissipation and Newtonian heating on boundary-layer flow of nanofluids over a flat plate. *International Journal of Numerical Methods for Heat and Fluid Flow* **23**(8): 1291–1303.
- Merkin J.H. 1986. On dual solutions occurring in mixed convection in a porous medium. *Journal of Engineering Mathematics* **20**: 171–179.
- Muhammad K., Hayat T. & Alsaedi A. 2021. Numerical study of Newtonian heating in flow of hybrid nanofluid (SWCNTs + CuO + Ethylene glycol) past a curved surface with viscous dissipation. *Journal of Thermal Analysis and Calorimetry* **143**: 1291–1302.
- Najib N., Bachok N., Arifin N.M. & Ali F.M. 2018. Stability analysis of stagnation-point flow in a nanofluid over a stretching / shrinking sheet with second-order slip, Soret and Dufour effects : A revised model. *Applied Sciences* **8**(4): 642.
- Patel V.K., Pandya J.U. & Patel M.R. 2023. Testing the influence of TiO<sub>2</sub>- Ag/water on hybrid nanofluid MHD flow with effect of radiation and slip conditions over exponentially stretching & shrinking sheets. *Journal of Magnetism and Magnetic Materials* **572**: 170591.
- Reddy S.R.R., Reddy P.B.A. & Suneetha S. 2018. Magnetohydro dynamic flow of blood in a permeable inclined stretching surface with viscous dissipation, non-uniform heat source/sink and chemical reaction. *Frontiers in Heat and Mass Transfer* **10**(1): 1-10.
- Vărdaru A., Humnic G., Humnic A., Fleacă C., Dumitrache F. & Morjan I. 2023. Aqueous hybrid nanofluids containing silver-reduced graphene oxide for improving thermo-physical properties. *Diamond and Related Materials* **132**: 109688.
- Waini I., Ishak A. & Pop I. 2019. Hybrid nanofluid flow and heat transfer past a permeable stretching/shrinking surface with a convective boundary condition. *Journal of Physics: Conference Series* **1366**: 012022.
- Weidman P.D., Kubitschek D.G. & Davis A.M.J. 2006. The effect of transpiration on self-similar boundary layer flow over moving surfaces. *International Journal of Engineering Science* **44**(11–12): 730–737.
- Zainal N.A., Nazar R., Naganthran K. & Pop I. 2020. MHD mixed convection stagnation point flow of a hybrid nanofluid past a vertical flat plate with convective boundary condition. *Chinese Journal of Physics* **66**: 630–644.

*Centre for Mathematical Sciences  
Universiti Malaysia Pahang Al-Sultan Abdullah  
Lebuhraya Persiaran Tun Khalil Yaakob  
26300 Kuantan,  
Pahang, MALAYSIA  
E-mail: rahimahj@umpsa.edu.my\*, mkhairulanuar@umpsa.edu.my*

*Faculty of Electrical & Electronics Engineering Technology  
Universiti Malaysia Pahang Al-Sultan Abdullah  
26600 Pekan,  
Pahang, MALAYSIA  
E-mail: hisyam@umpsa.edu.my*

Received: 22 May 2023

Accepted: 4 August 2023

---

\*Corresponding author